Coactivators necessary for transcriptional output of the hypoxia inducible factor, HIF, are directly recruited by ARNT PAS-B

Carrie L. Partch and Kevin H. Gardner[1]

Department of Biochemistry, University of Texas Southwestern Medical Center at Dallas, 5323 Harry Hines Boulevard, Dallas, TX 75390-8816

Edited by Peter E. Wright, The Scripps Research Institute, La Jolla, CA, and approved March 11, 2011 (received for review January 26, 2011)

Hypoxia-inducible factor (HIF) is the key transcriptional effector of the hypoxia response in eukaryotes, coordinating the expression of genes involved in oxygen transport, glycolysis, and angiogenesis to promote adaptation to low oxygen levels. HIF is a basic helix-loop-helix (bHLH)-PAS (PER-ARNT-SIM) heterodimer composed of an oxygen-labile HIF-α subunit and a constitutively expressed aryl hydrocarbon receptor nuclear translocator (ARNT) subunit, which dimerize via basic helix–loop–helix and PAS domains, and recruit coactivators via HIF-α C-terminal transactivation domains. Here we demonstrate that the ARNT PAS-B domain provides an additional recruitment site by binding the coactivator transforming acidic coiled-coil 3 (TACC3) in a step necessary for transcriptional responses to hypoxia. Structural insights from NMR spectroscopy illustrate how this PAS domain simultaneously mediates interactions with HIF-α and TACC3. Finally, mutations on ARNT PAS-B modulate coactivator selectivity and target gene induction by HIF in vivo, demonstrating a bifunctional role for transcriptional regulation by PAS domains within bHLH-PAS transcription factors.

transcriptional coactivators | protein/protein interactions | bifunctional interactions

Aryl hydrocarbon receptor nuclear translocator (ARNT) is the obligate heterodimeric partner for the basic helix–loop–helix (bHLH)-PAS (PER-ARNT-SIM) proteins aryl hydrocarbon receptor (AhR) and hypoxia-inducible factor-α (HIF-α), which serve as environmental sensors for xenobiotics and hypoxia, respectively (1). bHLH-PAS heterodimers are dependent on intersubunit contacts between the basic bHLH and tandem PAS domains (2–4). The second of two PAS domains, PAS-B, plays a critical role in maintaining the stability of this complex, given that mutations in HIF-2α PAS-B disrupt HIF-α/ARNT interactions and decrease transactivation in vivo (3, 4). Therefore, our current model of bHLH-PAS heterodimer architecture is based on nucleation of the core transcription factor complex by bHLH and PAS domains, leaving C-terminal transactivation domains (TADs) to recruit coactivator proteins that are required for gene regulation (Fig. 1*A*).

Further study of HIF TADs reveals that not all are essential for HIF function. In particular, deletion of the putative ARNT C-terminal TAD has a minimal effect on transactivation of endogenous targets (5–7), whereas deletion of the two HIF-α TADs (N-TAD and C-TAD) eliminates hypoxia-induced transactivation (8). Consequently, study of HIF transcriptional regulation has focused on the HIF-α TADs, identifying the C-TAD as the primary site of recruitment for p300/CBP (9) and the N-TAD as a determining factor in the distinctive profiles of target gene induction by HIF-1α and HIF-2α (10). Selectivity is mediated in part by the recruitment of different coactivators by the N-TADs of the two HIF-α isoforms, building on an emerging theme that transcriptional coregulators and promoter context influence the specificity of gene induction by transcription factors (11, 12). Domain-swapping studies have shown that PAS domains also contribute to the selectivity of target gene induction within the bHLH-PAS family (13), suggesting that other mechanisms for regulating transcriptional activity exist aside from the C-terminal TADs. Within HIF, ARNT PAS-B interacts with coactivators (TRIP230 and CoCoA) that are required for transcriptional

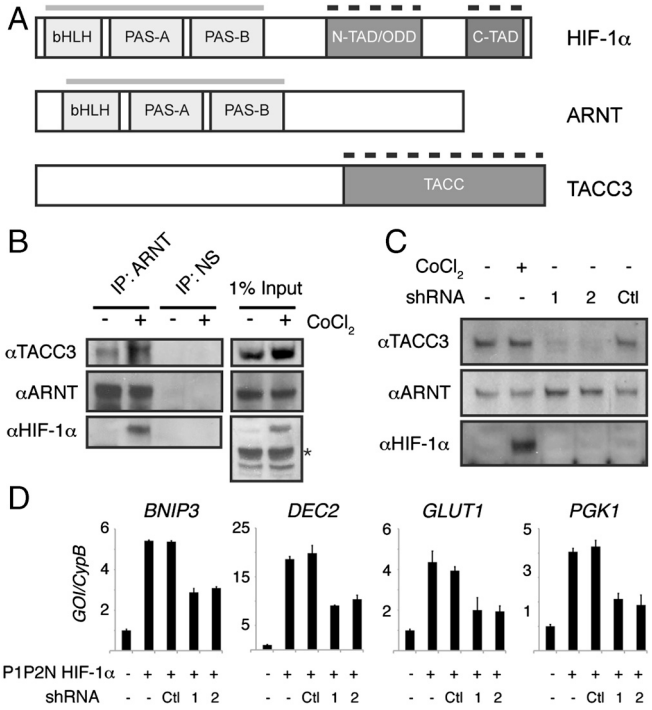

Fig. 1. *TACC3 interacts with ARNT to regulate HIF transactivation.* (*A*) Domain organization of HIF-1α, ARNT, and TACC3. Gray bars indicate domains of the bHLH-PAS proteins that mediate heterodimerization; dashed black bars indicate domains that interact with other transcriptional coregulators. (*B*) TACC3 coimmunoprecipitates with ARNT. HEK 293T cells were treated with 200 μM $CoCl_2$ for 16 h prior to harvest. Antibodies to ARNT and a nonspecific (NS) control (GAL4 DNA-binding domain) were used to immunoprecipitate complexes from whole-cell lysates. Asterisk, nonspecific band. (*C*) Immunoblot analysis of whole-cell lysates for TACC3 expression from 293T cells harvested after $CoCl_2$ (200 μM, 16 h) or transfected with shRNA vectors (48 h). (*D*) QPCR analysis of HIF target genes from 293T cells harvested 48 h after transfection with indicated plasmids. Expression levels were all normalized by dividing expression of the gene of interest by an internal standard cyclophilin B (*GOI/CypB*).

Author contributions: C.L.P. and K.H.G. designed research; C.L.P. performed research; C.L.P. and K.H.G. analyzed data; and C.L.P. and K.H.G. wrote the paper.

The authors declare no conflict of interest.

This article is a PNAS Direct Submission.

[1]To whom correspondence should be addressed. E-mail: Kevin.Gardner@UTSouthwestern.edu.

This article contains supporting information online at www.pnas.org/lookup/suppl/doi:10.1073/pnas.1101357108/-/DCSupplemental.

responses to hypoxia and xenobiotics (14–16). These data strongly suggest that ARNT plays a more active role in HIF transactivation than simply providing a platform for HIF-α heterodimerization.

TRIP230 and CoCoA are joined by a third coactivator, transforming acidic coiled-coil 3 (TACC3), that has also been implicated as a coactivator for HIF via specific interactions with ARNT and ARNT2 but not HIF-1α (17). TACC3 is an Epo-inducible member of the TACC family (18), all of which share an approximately 200 residue dimeric C-terminal coiled-coil domain that interacts with numerous transcription factors and chromatin-modifying proteins (Fig. 1*A*) (19). Here we identify the molecular basis for TACC3 regulation of HIF transactivation, mediated by a direct interaction with ARNT PAS-B that utilizes an interface shared with TRIP230 and CoCoA. Using solution NMR mapping and mutagenesis studies to create a model of the heterotrimeric complex, we demonstrate how the modular ARNT PAS-B domain simultaneously engages its heterodimeric HIF-α partner and TACC3. Notably, ARNT PAS-B point mutations alter selectivity for coactivators and lead to changes in the profile of endogenous target gene induction.

Results

TACC3 Interacts with ARNT to Regulate HIF-Dependent Transcription. Following up on a previous report that TACC3 interacts with ARNT in vitro (17), we immunoprecipitated endogenous ARNT from human embryonic kidney 293T (293T) cells under normoxic conditions in the absence and presence of the hypoxia-mimetic $CoCl_2$, which stabilizes HIF-1α protein by inhibiting oxygen-dependent hydroxylases that normally induce degradation (20). We detected a hypoxia-independent interaction of TACC3 with ARNT, demonstrating that HIF-1α binding is not required (Fig. 1*B*). We also noted a modest increase in TACC3 protein upon stabilization of endogenous HIF-1α by $CoCl_2$ that was validated at the mRNA level by quantitative PCR (QPRC) (Fig. S1*A*), suggesting that HIF may regulate TACC3 expression directly or indirectly. To investigate the role of TACC3 in HIF transactivation, we depleted TACC3 (Fig. 1*C* and Fig. S1*A*) and monitored expression of four endogenous HIF-1 target genes (*BNIP3*, *DEC2*, *GLUT1*, and *PGK1*) by QPCR (Fig. 1*D*). Depletion of TACC3 significantly decreased expression of all four genes, demonstrating that TACC3 is a HIF-1 coactivator in vivo. TACC3 depletion also significantly decreased the activation of a *VEGF* hypoxia response element luciferase reporter construct (*VEGF* HRE:luc) (21) by HA-P1P2N HIF-1α or HIF-2α proteins, constitutively active forms of HIF-α that are no longer subject to oxygen-dependent hydroxylation (Fig. S1*B*) (22). These data show that TACC3 can act as a coactivator for both HIF-1 and HIF-2 complexes, consistent with recruitment of TACC3 by the ARNT subunit in both complexes. Importantly, we confirmed previous reports that transactivation by HIF-2 absolutely requires the HIF-2α TADs (Fig. S1*C*) (10), suggesting that coactivators recruited by both HIF-α and ARNT are both necessary for complete HIF transactivation.

Interaction Sites on Both ARNT PAS-B and TACC3 Are Shared with Other Transcriptional Coregulators. While it is known that ARNT and TACC3 interact, this was established with a relatively large fragment of ARNT (approximately 450 residues) encompassing both of its PAS domains (17). To determine if one of the PAS domains specifically mediates the interaction, we performed pull-down assays with purified, isolated His_6-tagged ARNT PAS-A and PAS-B constructs and a GST-tagged 324 residue TACC3 fragment representing the ARNT-interacting fragment isolated from the yeast two-hybrid screen. As with the other coiled-coil coactivators TRIP230 and CoCoA, the ARNT PAS-B domain was sufficient to interact directly with TACC3, whereas the PAS-A domain showed negligible coactivator binding (Fig. 2*A*) (16).

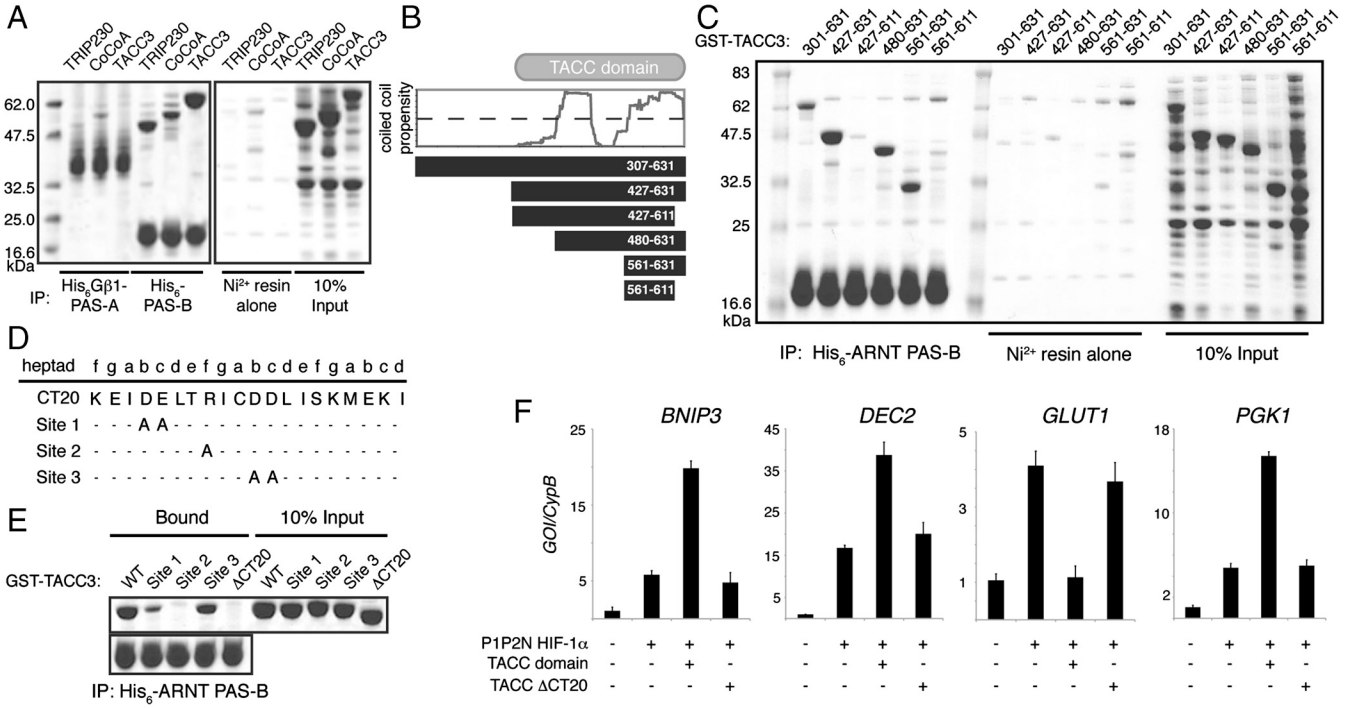

Fig. 2. *A common interface in the C terminus of TACC3 mediates interaction with ARNT and other transcriptional regulators.* (*A*) Ni-pulldown assay using purified His_6-Gβ1-ARNT PAS-A or His_6-ARNT PAS-B with soluble *E. coli* extracts containing overexpressed GST-tagged coactivators. (*B*) Illustration of various TACC3 truncations used in this study. Dashed line represents significance cutoff for coiled-coil analysis. (*C*) Ni-pulldown assay of His_6-ARNT PAS-B with GST-TACC3 fragments. (*D*) Identification of CT20 mutants previously identified to disrupt TACC3 binding to FOG-1 (23). (*E*) Ni-pulldown assay of His_6-ARNT PAS-B with mutant GST-TACC3 fragments. (*F*) QPCR analysis of HIF target genes from 293T cells harvested 48 h after transfection with indicated plasmids. Error bars, SD for $n = 3$ independent biological replicates.

Therefore, ARNT PAS-B provides a common site for recruiting diverse coiled-coil transcriptional coactivators to the HIF heterodimer, in addition to its critical role in maintaining this complex via interaction with HIF-α PAS-B domains.

To identify where ARNT binds TACC3, we made a series of truncations of the C-terminal TACC domain based on secondary structure and coiled-coil predictions (Fig. 2*B*). We were particularly interested in the role of the C-terminal 20 residues (CT20) in the ARNT/TACC3 interaction, because these residues are critical for TACC3 binding to the transcriptional coregulator FOG-1 (friend of GATA-1) (23). Using pulldown assays with His_6-tagged ARNT PAS-B, we determined that a C-terminal fragment of the GST-TACC domain (residues 561–631) was sufficient to interact with ARNT PAS-B (Fig. 2*C*). As observed with FOG-1, this binding was dependent on the CT20. To further test the nature of this interface, we made point mutations on the exposed face of the coiled-coil dimer within the CT20 (Fig. 2*D*) that were also shown to disrupt the interaction with FOG-1 (23). All three mutants reduced ARNT binding (Fig. 2*E*), but most effectively with the R619A mutant. This mutation specifically disrupts the ARNT/TACC3 interaction without global effects on TACC3 structure (Fig. S2*A*). These data demonstrate that TACC3 utilizes a common site within its CT20 region to interact with ARNT PAS-B and at least one other transcriptional regulator.

We then asked whether the isolated TACC domain was capable of stimulating HIF-1 transactivation. The TACC domain stimulated a twofold to fourfold increase in HIF-1-dependent expression of *BNIP3*, *DEC2*, and *PGK* (Fig. 2*F*) or the *VEGF* HRE : luc reporter (Fig. S2*B*) that was dependent on the presence of the CT20. Interestingly, the TACC domain had the opposite effect on transcription of the *GLUT1* gene, eliminating the HIF-1-dependent up-regulation of mRNA levels. Given that knockdown of TACC3 decreased *GLUT1* transcription (Fig. 1*C*), suggesting that it positively regulates the *GLUT1* gene, these data imply that modest overexpression of the isolated TACC domain competes with another important coactivator that is specifically required for *GLUT1* expression, analogous to squelching (24, 25).

Biochemical Basis of Selectivity for TACC Family Binding by ARNT PAS-B. The TACC domain is the identifying feature of the TACC family, with a high degree of homology between TACC3 and other members such as TACC1, TACC2, and even *Drosophila* TACC (Fig. S3). Based on this conservation, particularly within CT20 (Fig. 3*A*), we reasoned that all three mammalian TACC family members might interact with ARNT PAS-B. Using analogous fragments containing the last 70 residues of GST-TACC1, GST-TACC2, and GST-TACC3, we assayed for ARNT PAS-B binding by pulldown assay and found that only GST-TACC3 bound (Fig. 3*B*). A closer investigation of the TACC CT20 alignment showed modest differences between the three isoforms within the C-terminal 6 residues (CT6). Truncation of the CT6 residues abrogated TACC3 binding in vitro (Fig. 3*C*), so we investigated whether swapping the C termini of TACC1 and TACC3 would be sufficient to confer selectivity for ARNT. Swapping the TACC1 C terminus (T1-CT) for that of TACC3 still permitted binding of the chimeric GST-TACC3 protein to ARNT PAS-B and conversely, the TACC3 CT (T3-CT) was not sufficient to confer binding to the GST-TACC1 chimera (Fig. 3*C*). These data demonstrate that although residues within the TACC3 CT6 are critical for binding, the specific determinant(s) of ARNT binding by TACC3 are further upstream in the CT20 region.

Within the sequence upstream of the CT6 region, there is nearly 90% identity between the mammalian TACC family (Fig. 3*A*). The Q711K/K718R GST-TACC1 double mutant, designed to mimic residues conserved in mammalian TACC3 genes, was insufficient to restore binding in the pulldown assay; however, addition of E722D to this double mutant facilitated interaction of GST-TACC1 (Q711K/K718R/E722D) with ARNT PAS-B (Fig. 3*D*). The E772D mutation alone was sufficient to alter TACC selectivity and allow binding of GST-TACC1 (E722D) to ARNT PAS-B. We tested whether this held true for GST-TACC2 by making the analogous mutation (E2940D) and demonstrated that it was also sufficient to restore interaction with ARNT PAS-B; conversely, the opposing D623E mutation in GST-TACC3 disrupted the interaction (Fig. 3*D*). These data show that the basis of TACC family selectivity for direct binding to the ARNT PAS-B domain is based upon a highly conserved switch from glutamate (TACC1, 2) to aspartate (TACC3).

Structural Model of the HIF-2α/ARNT/TACC3 Complex. Having defined the biochemical basis for the TACC3/ARNT interaction, we used solution NMR experiments to determine where TACC3 binds on the surface of ARNT PAS-B. In these experiments, we titrated a shorter C-terminal coiled-coil fragment of TACC3 (Fig. S4 *A* and *B*) into uniformly ^{15}N-labeled ARNT PAS-B, using 2D $^{15}N/^{1}H$ HSQC spectra to monitor binding. Select cross-peaks within these $^{15}N/^{1}H$ HSQC spectra exhibited significant TACC3-dependent broadening, or loss of signal intensity, consistent with formation of the complex with intermediate exchange kinetics (Fig. 4*A* and Fig. S4*C*). Significantly perturbed residues were identified by differential broadening analysis (Fig. S4*D*) and mapped onto the ARNT PAS-B structure, defining an interface on the α-helical surface of the PAS-B domain (Fig. 4*B*). Given the similarity of this TACC3-binding interface to the binding sites we previously observed by NMR for the coiled-coil coactivators TRIP230 and CoCoA (16), we asked whether the coactivators could compete for binding ARNT PAS-B in vitro. Consistent with their shared interface on ARNT PAS-B, increasing amounts of GST-TACC3 decreased binding of GST-TRIP230 to ARNT PAS-B, whereas a nonbinding GST-tagged control protein had little effect (Fig. S4*E*).

To generate a structural model illustrating how ARNT PAS-B recruits TACC3 to this common binding site while simultaneously binding its HIF-α PAS-B partner, we used an experimentally

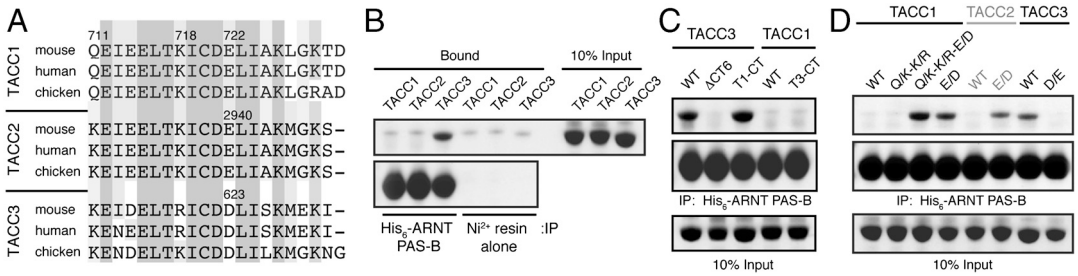

Fig. 3. *ARNT selectivity for TACC3 is mediated by a conservative amino acid change within the TACC family.* (*A*) Sequence alignment of TACC family CT20 residues. Residues mutated in *D* are indicated with numbering with respect to human TACC genes. (*B*) Ni-pulldown assay of His_6-ARNT PAS-B with GST-TACC family fragments. (*C*) Ni-pulldown assay of His_6-ARNT PAS-B with GST-TACC CT-swap and truncation fragments. (*D*) Ni-pulldown assay of His_6-ARNT PAS-B with GST-TACC mutants.

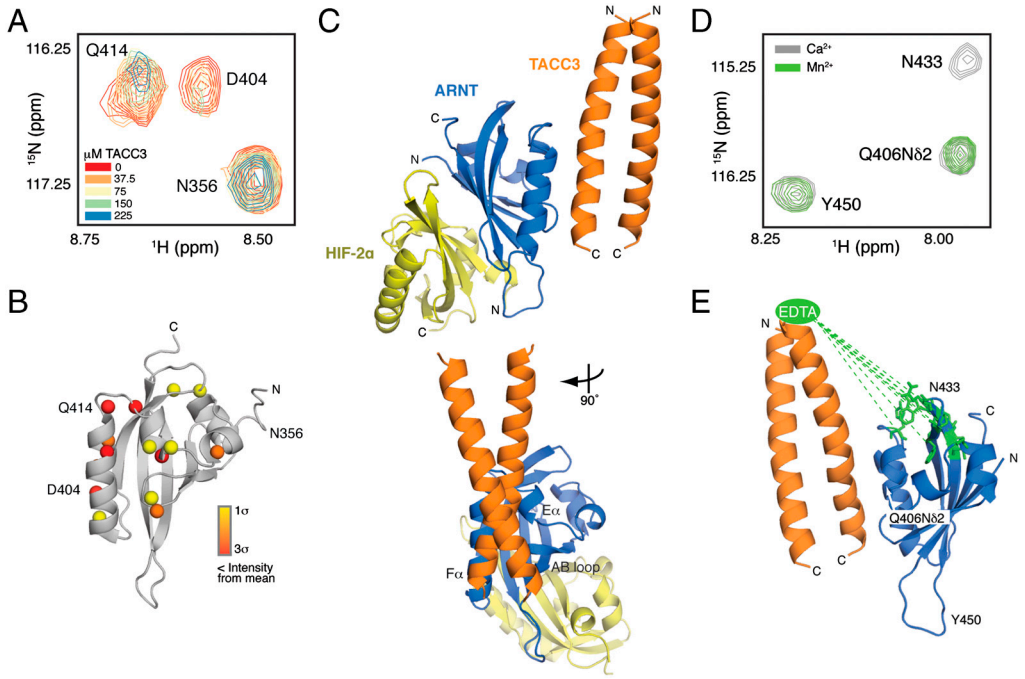

Fig. 4. *Structural basis for TACC3 recruitment by ARNT PAS-B.* (*A*) Close-up view of broadened residues within the ^{15}N/^{1}H HSQC spectra of ^{15}N ARNT PAS-B titrated with natural abundance TACC3. (*B*) Significantly perturbed amide protons heat-mapped onto the ARNT PAS-B structure [Protein Data Bank (PDB) ID code 1XO0 (40)] as spheres according to degree of broadening. (*C*) HADDOCK model depicting simultaneous engagement of HIF-2α PAS-B (yellow) and the TACC3 C terminus (orange) by ARNT PAS-B (blue). (*D*) Close-up view of broadened residues within the ^{15}N/^{1}H HSQC spectra of ^{15}N ARNT PAS-B with EDTA-derivatized TACC3 (M598C) chelated with either Ca^{2+} (gray) or Mn^{2+} (green). (*E*) Broadened residues mapped onto the ARNT PAS-B structure [PDB ID code 1XO0 (40)] in green, with dashed line showing approximately 28–35 Å distance from location of covalently attached EDTA moiety.

guided molecular docking approach. Using a high-resolution structure of the ARNT PAS-B/HIF-2α PAS-B heterodimer (26) and a de novo model of the TACC3 C-terminal coiled coil validated by experimental studies (23) (Fig. S4*B*), we used a semirigid body docking algorithm implemented within the HADDOCK program (27). These calculations generated ternary complexes that were scored for their ability to satisfy a combination of experimental data (derived from NMR mapping and biochemical data) and empirical distance restraints, identifying a single low energy complex that satisfied these data much better than all alternatives (Fig. 4*C* and Fig. S5*A*; coordinates provided in Dataset S1). This ternary complex positions TACC3 onto an interface provided by the Eα and Fα helices of ARNT, together with a portion of the AB loop. This interaction buries approximately 980 Å^2, consistent with the moderate affinity of the interaction, and relies on chiefly polar interactions between residues on both sides of the complex (Fig. S5*B*). By relegating interactions with the HIF-α PAS-B and coactivators to opposing sides of this 14-kDa domain, ARNT PAS-B can play a critical role in both the stability of the core HIF heterodimer and in its transactivation function via coactivator recruitment.

To validate this model, we used paramagnetic relaxation enhancement data from NMR experiments to obtain unique distance and orientational restraints. Point mutations at two sites (M598C and M605C) on TACC3, located approximately 28–40 Å N-terminal to residue D623 on the ARNT-binding surface of TACC3, allowed us to covalently derivatize TACC3 with an S-cysteaminyl-EDTA moiety that facilitated coordination of divalent cations. The effects of derivatized TACC3 on ^{15}N ARNT PAS-B were monitored by ^{15}N/^{1}H HSQC spectra and used to identify residues significantly perturbed by paramagnetic Mn^{2+}EDTA-TACC3 relative to the inert Ca^{2+}EDTA-TACC3 (Fig. 4 *D* and Fig. S5 *C* and *D*). These residues cluster on one end of the ARNT PAS-B domain (Fig. 4*E*), consistent with the expected distance from the chelated metals and orientation of TACC3 observed in our HADDOCK model.

Mutations in ARNT PAS-B Perturb Coactivator Binding and HIF Transactivation. To validate the interfacial residues identified in the HADDOCK model, we made point mutations in the ARNT PAS-B AB loop (E370R), Eα (E398M), and Fα (K417W) helices that were predicted to disrupt the TACC3 interaction (Fig. 5*A*). Recombinant mutant proteins were well folded with chemical shift changes localized to the site of mutation (Fig. S6 *A–C*), demonstrating selective perturbation of the coactivator binding interface on ARNT PAS-B. We tested each of the His_6-ARNT PAS-B mutants for binding to GST-TACC3 and GST-TRIP230 by pulldown assay (Fig. 5*B*) and measured the effect of mutations on complex formation by densitometric analysis of bound complexes (Fig. 5*C* and Fig. S6 *D* and *E*). Mutations E370R and E398M, located at the center of the ARNT/TACC3 interface, decreased complex formation with both GST-TACC3 and GST-TRIP230 (Fig. 5 *B* and *C*). The Fα helix K417W mutant, located at the edge of the ARNT/TACC3 interface, decreased complex formation with GST-TACC3 2.7-fold while increasing formation of the GST-TRIP230/His_6-ARNT PAS-B (K417W) complex by nearly 3-fold, resulting in an apparent 8-fold change in coactivator selectivity.

To determine whether point mutations that alter coactivator binding in vitro could affect ARNT function in vivo, we quantified activation of HIF-1 target genes in the presence of wild-type or mutant FLAG-ARNT. Expression of the E370R or E398M mutants, which decreased complex formation with both TACC3 and TRIP230 in vitro, led to a significant decrease in the transcription of the four genes that we assayed (Fig. 5*D*). In contrast, these genes were differentially affected by the K417W mutant that displayed changes in coactivator selectivity in vitro. Although K417W induced expression of *BNIP3*, *DEC2*, and *PGK1* or a VEGF HRE:luc reporter comparable to that of wild-type ARNT

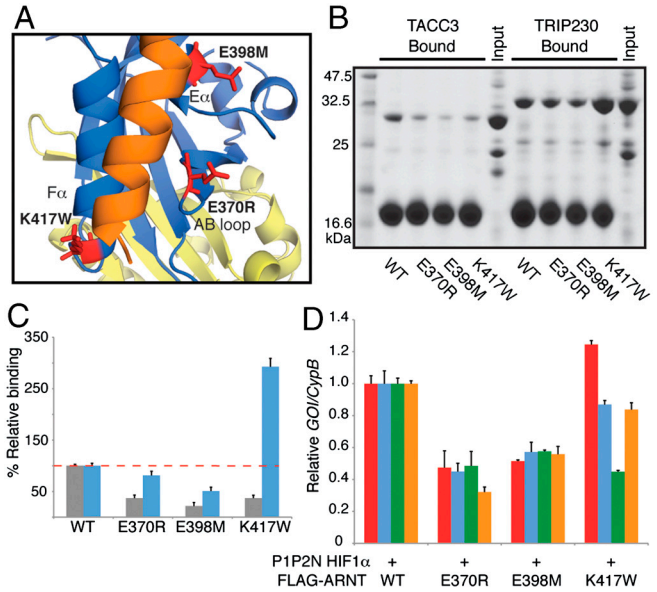

Fig. 5. *Mutations on ARNT PAS-B alter coactivator selectivity and HIF activation*. (*A*) Close-up view of HADDOCK model illustrating ARNT PAS-B/TACC3 interface with ARNT PAS-B mutants shown in red. (*B*) Ni-pulldown assay of His_6-ARNT PAS-B WT and mutants with GST-TACC3 or GST-TRIP230. (*C*) Densitometric analysis of bound GST-TACC3 (gray) or GST-TRIP230 (blue) with WT and mutant His_6-ARNT PAS-B. (*D*) QPCR analysis of HIF target genes from 293T cells harvested 48 h after transfection with indicated plasmids. *BNIP3*, red; *DEC2*, blue; *GLUT1*, green; *PGK1*, orange. Data are normalized to individual target gene expression in the presence of WT FLAG-ARNT. Error bars, SD for $n = 3$ independent biological replicates.

(Fig. 5*D* and Fig. S6 *F* and *G*), the mutant was not able to drive normal levels of *GLUT1* transcription. These results are consistent with our data suggesting a unique role for TACC3 at the *GLUT1* promoter (Fig. 2*F*), supporting a model where TACC3 recruitment by ARNT PAS-B plays an indispensable role in transcriptional regulation of this gene and possibly others by HIF.

Discussion

HIF-1α and HIF-2α protein levels serve as a readout of cellular oxygen tension due to the tight control of their stability by oxygen-dependent hydroxylation and subsequent proteosomal degradation (28). Formation of the HIF heterodimer with ARNT is required for cellular adaptation to hypoxia, facilitating anaerobic metabolism, erythropoiesis, and angiogenesis through the up-regulation of over 100 genes (29). Either because of its constitutive expression or the lack of a potent C-terminal TAD on ARNT, not much attention has been focused on how, or if, it contributes to transactivation of HIF. This study provides insight into the molecular architecture of bHLH-PAS transcription factors and reveals the important role that an ARNT PAS domain plays in the HIF transcription factor complex. By mediating simultaneous interactions with its HIF-α partners and coactivators, ARNT PAS-B plays an essential role in both the architecture and activation of HIF complexes.

Notably, although coactivator recruitment by ARNT PAS-B is important for maximal HIF transactivation, it is insufficient to drive transcription in the absence of HIF-α TADs, suggesting the existence of functional interplay between coactivators recruited by the two HIF subunits. Our study adds another level of complexity to HIF transcriptional regulation by underscoring the importance of the ARNT PAS-B domain to simultaneously bind the HIF-α PAS-B domain and directly recruit coiled-coil coactivator proteins. Future studies will help define the factors that regulate recruitment of specific coactivators to ARNT, as well as clarify the role that these coactivators play in transactivation of other ARNT-containing complexes such as the bHLH-PAS AhR/ARNT heterodimer, which regulates transcriptional responses to xenobiotics.

Despite significant sequence conservation in the ARNT-binding region of mammalian TACC family proteins, we showed that only TACC3 could interact directly with ARNT (Fig. 3). We found that the presence of an additional methylene group on the side chain at position 623 in TACC3, changing from an aspartate to glutamate, was responsible for the loss of ARNT binding by TACC1 and TACC2. Our model of the ARNT PAS-B/TACC3 complex indicates that D623 is located in the core of the interface with ARNT (Fig. S5*B*), suggesting that D623E mutant may lead to steric clashes between the two proteins. Consistent with this, the D623A mutant was still capable of interacting with ARNT PAS-B (Fig. 2*E*). Although a high-resolution structure of the complex is needed to resolve the ARNT PAS-B/TACC3 interface in better detail, our data demonstrate that the C terminus of TACC3 is clearly necessary to tether the rest of the TACC domain to the HIF complex via the ARNT PAS-B domain.

Deletion of *TACC3* in mice causes embryonic lethality in mid to late gestation with profound defects in hematopoietic stem cell populations, demonstrating that it has an essential and nonredundant function within the TACC family (30). One manner in which TACC3 regulates hematopoiesis is through a direct interaction with FOG-1, a transcriptional coregulator of the master erythroid transcription factor GATA-1. TACC3 regulates GATA-1 transcriptional activity by competing for interaction with FOG-1 in a regulatory squelching mechanism that retards terminal erythroid differentiation (31). We show here that TACC3 utilizes the same protein interface within its C-terminal 20 residues to interact with ARNT PAS-B and FOG-1 (23) (Fig. 2 and Fig. S7).

Notably, the hematopoietic defects in *TACC3*-/- embryos are phenotypically similar to *HIF-1*α, *HIF-2*α, and *ARNT* knockout embryos (30, 32–36). HIF activation by hypoxic niches within bone marrow is critically important for controlling the fate of hematopoietic stem cells and their progeny, orchestrating a balance of quiescence, self-renewal, differentiation, and apoptosis (37, 38). Because *TACC3*-/- embryos exhibit dramatically reduced hematopoietic stem cell colony formation activity (approximately 1–5% of WT) (30), we propose that loss of TACC3 may compromise HIF activity and regulation of hematopoietic stem cell fate. A similar role was also recently reported for TACC3 and ARNT2 in neuronal progenitor cells. Disruption of the TACC3/ARNT2 interaction by a small molecule inhibitor accelerated differentiation within neural progenitor cells (39), suggesting that the ARNT PAS-B mediated interaction described here may play an important role in mediating cell fate decisions by several types of stem cell populations.

Methods

Pulldown assays. His_6-tagged ARNT PAS domains were purified as described in *SI Methods*. Proteins were incubated at 5 μM with GST-tagged coactivators in soluble *Escherichia coli* extract (15 μM coactivator) and Ni-NTA agarose (Qiagen) in 50 mM Tris pH 7.5, 150 mM NaCl, 20 mM imidazole, and 10 mM β-mercaptoethanol for 4 h at 4 °C. Samples were washed twice with 0.5 mL of the same buffer and eluted with 2× SDS buffer. Bound proteins were resolved by SDS-PAGE and Coomassie stained. Densitometric quantification of bound proteins was performed using ImageJ (National Institutes of Health) from three independent experiments with SD shown.

mRNA Quantification. Total RNA was extracted from transfected HEK293T cells using Trizol (Invitrogen) according to the manufacturer's instructions. cDNA was synthesized from 1 ug RNA using the iScript cDNA Synthesis kit (Bio-Rad), and gene expression was analyzed from 1 μg cDNA by quantitative PCR using iTaq SYBR green Supermix with ROX on a CFX96 Real Time System (Bio-Rad). QPCR primer details are available in *SI Materials*. The results of triplicate experiments are expressed as $2^{(-\Delta\Delta C_T)}$ with SE shown, where the average Ct of the gene of interest after treatment was normalized to the reference

gene, *Cyclophilin B*, and compared to a normalized, untreated sample for fold change.

NMR Spectroscopy. NMR experiments were conducted at 25 °C using a Varian INOVA 600-MHz spectrometer equipped with ^{1}H, ^{13}C, ^{15}N triple resonance, *Z*-axis pulsed field gradient probes. Differential broadening analysis of $^{15}N/^{1}H$ HSQC experiments for TACC3 binding and paramagnetic relaxation enhancement were carried out as before (16), using chemical shift assignments of wild-type ARNT PAS-B (40) and peak intensities of 150 μM ^{15}N ARNT PAS-B in the presence of 150 μM TACC3-CT.NMR data were processed using NMRPipe/NMRDraw (41) and analyzed with NMRViewJ (42).

HADDOCK Modeling. A TACC3 C-terminal peptide (residues 601–631) was modeled as a parallel coiled-coil dimer using Rosetta (43). Complexes with the crystallographic ARNT PAS-B/HIF-2α PAS-B heterodimer [PDB ID code 3F1P (26)] were docked using the HADDOCK2.0 Web server (27). Residues used for docking are listed in *SI Methods*. The protocol for docking and refining followed default parameters, including semiflexible simulated annealing of all proteins in the 200 lowest-intermolecular energy solutions followed by refinement in explicit water.

ACKNOWLEDGMENTS. We thank Dr. Joseph Garcia (University of Texas Southwestern Medical Center, Dallas, TX) for the HA-P1P2N-HIF-1α and HIF-2α plasmids, Dr. Richard Bruick (University of Texas Southwestern Medical Center, Dallas, TX) for the *VEGF* HRE:luc plasmid, and Laura Davidson for assistance with these studies. This study was supported by National Institutes of Health Grant GM081875 (to K.H.G.) and Grant CA130441 (to C.L.P.). C.L.P. was also supported by a fellowship from the A. L. Chilton Foundation.

1. Kewley RJ, Whitelaw ML, Chapman-Smith A (2004) The mammalian basic helix-loop-helix/PAS family of transcriptional regulators. *Int J Biochem Cell Biol* 36:189–204.
2. Chapman-Smith A, Lutwyche JK, Whitelaw ML (2004) Contribution of the Per/Arnt/Sim (PAS) domains to DNA binding by the basic helix-loop-helix PAS transcriptional regulators. *J Biol Chem* 279:5353–5362.
3. Erbel PJ, Card PB, Karakuzu O, Bruick RK, Gardner KH (2003) Structural basis for PAS domain heterodimerization in the basic helix–loop–helix-PAS transcription factor hypoxia-inducible factor. *Proc Natl Acad Sci USA* 100:15504–15509.
4. Yang J, et al. (2005) Functions of the Per/ARNT/Sim domains of the hypoxia-inducible factor. *J Biol Chem* 280:36047–36054.
5. Hoffman EC, et al. (1991) Cloning of a factor required for activity of the Ah (dioxin) receptor. *Science* 252:954–958.
6. Ko HP, Okino ST, Ma Q, Whitlock JP, Jr (1996) Dioxin-induced CYP1A1 transcription in vivo: The aromatic hydrocarbon receptor mediates transactivation, enhancer-promoter communication, and changes in chromatin structure. *Mol Cell Biol* 16:430–436.
7. Li H, Ko HP, Whitlock JP (1996) Induction of phosphoglycerate kinase 1 gene expression by hypoxia. Roles of Arnt and HIF1alpha. *J Biol Chem* 271:21262–21267.
8. Jiang BH, Zheng JZ, Leung SW, Roe R, Semenza GL (1997) Transactivation and inhibitory domains of hypoxia-inducible factor 1alpha. Modulation of transcriptional activity by oxygen tension. *J Biol Chem* 272:19253–19260.
9. Ruas JL, Poellinger L, Pereira T (2002) Functional analysis of hypoxia-inducible factor-1 alpha-mediated transactivation. Identification of amino acid residues critical for transcriptional activation and/or interaction with CREB-binding protein. *J Biol Chem* 277:38723–38730.
10. Hu CJ, et al. (2006) Differential regulation of the transcriptional activities of hypoxia-inducible factor 1 alpha (HIF-1alpha) and HIF-2alpha in stem cells. *Mol Cell Biol* 26:3514–3526.
11. McKenna NJ, Nawaz Z, Tsai SY, Tsai MJ, O'Malley BW (1998) Distinct steady-state nuclear receptor coregulator complexes exist in vivo. *Proc Natl Acad Sci USA* 95:11697–11702.
12. Ravnskjaer K, et al. (2007) Cooperative interactions between CBP and TORC2 confer selectivity to CREB target gene expression. *EMBO J* 26:2880–2889.
13. Zelzer E, Wappner P, Shilo BZ (1997) The PAS domain confers target gene specificity of Drosophila bHLH/PAS proteins. *Genes Dev* 11:2079–2089.
14. Beischlag TV, et al. (2004) Recruitment of thyroid hormone receptor/retinoblastoma-interacting protein 230 by the aryl hydrocarbon receptor nuclear translocator is required for the transcriptional response to both dioxin and hypoxia. *J Biol Chem* 279:54620–54628.
15. Kim JH, Stallcup MR (2004) Role of the coiled-coil coactivator (CoCoA) in aryl hydrocarbon receptor-mediated transcription. *J Biol Chem* 279:49842–49848.
16. Partch CL, Card PB, Amezcua CA, Gardner KH (2009) Molecular basis of coiled coil coactivator recruitment by the aryl hydrocarbon receptor nuclear translocator (ARNT). *J Biol Chem* 284:15184–15192.
17. Sadek CM, et al. (2000) Isolation and characterization of AINT: A novel ARNT interacting protein expressed during murine embryonic development. *Mech Dev* 97:13–26.
18. McKeveney PJ, et al. (2001) Characterization and localization of expression of an erythropoietin-induced gene, ERIC-1/TACC3, identified in erythroid precursor cells. *Br J Haematol* 112:1016–1024.
19. Peset I, Vernos I (2008) The TACC proteins: TACC-ling microtubule dynamics and centrosome function. *Trends Cell Biol* 18:379–388.
20. Metzen E, et al. (2003) Intracellular localisation of human HIF-1 alpha hydroxylases: Implications for oxygen sensing. *J Cell Sci* 116:1319–1326.
21. Tian H, McKnight SL, Russell DW (1997) Endothelial PAS domain protein 1 (EPAS1), a transcription factor selectively expressed in endothelial cells. *Genes Dev* 11:72–82.
22. Dioum EM, et al. (2009) Regulation of hypoxia-inducible factor 2alpha signaling by the stress-responsive deacetylase sirtuin 1. *Science* 324(5932):1289–1293.
23. Simpson RJ, et al. (2004) A classic zinc finger from friend of GATA mediates an interaction with the coiled-coil of transforming acidic coiled-coil 3. *J Biol Chem* 279:39789–39797.
24. Ablack JN, et al. (2010) Comparison of E1A CR3 dependent transcriptional activation across six different human adenovirus subgroups. *J Virol* 84:12771–12781.
25. He B, et al. (2008) A repressive role for prohibitin in estrogen signaling. *Mol Endocrinol* 22:344–360.
26. Scheuermann TH, et al. (2009) Artificial ligand binding within the HIF2alpha PAS-B domain of the HIF2 transcription factor. *Proc Natl Acad Sci USA* 106:450–455.
27. de Vries SJ, van Dijk M, Bonvin AM (2010) The HADDOCK web server for data-driven biomolecular docking. *Nat Protoc* 5:883–897.
28. Kaelin WG, Jr, Ratcliffe PJ (2008) Oxygen sensing by metazoans: The central role of the HIF hydroxylase pathway. *Mol Cell* 30:393–402.
29. Semenza GL (2003) Targeting HIF-1 for cancer therapy. *Nat Rev Cancer* 3:721–732.
30. Piekorz RP, et al. (2002) The centrosomal protein TACC3 is essential for hematopoietic stem cell function and genetically interfaces with p53-regulated apoptosis. *EMBO J* 21:653–664.
31. Garriga-Canut M, Orkin SH (2004) Transforming acidic coiled-coil protein 3 (TACC3) controls friend of GATA-1 (FOG-1) subcellular localization and regulates the association between GATA-1 and FOG-1 during hematopoiesis. *J Biol Chem* 279:23597–23605.
32. Adelman DM, Maltepe E, Simon MC (1999) Multilineage embryonic hematopoiesis requires hypoxic ARNT activity. *Genes Dev* 13:2478–2483.
33. Iyer NV, et al. (1998) Cellular and developmental control of O2 homeostasis by hypoxia-inducible factor 1 alpha. *Genes Dev* 12:149–162.
34. Peng J, Zhang L, Drysdale L, Fong GH (2000) The transcription factor EPAS-1/hypoxia-inducible factor 2alpha plays an important role in vascular remodeling. *Proc Natl Acad Sci USA* 97:8386–8391.
35. Ramirez-Bergeron DL, Runge A, Adelman DM, Gohil M, Simon MC (2006) HIF-dependent hematopoietic factors regulate the development of the embryonic vasculature. *Dev Cell* 11:81–92.
36. Ryan HE, Lo J, Johnson RS (1998) HIF-1 alpha is required for solid tumor formation and embryonic vascularization. *EMBO J* 17:3005–3015.
37. Simsek T, et al. (2010) The distinct metabolic profile of hematopoietic stem cells reflects their location in a hypoxic niche. *Cell Stem Cell* 7:380–390.
38. Takubo K, et al. (2010) Regulation of the HIF-1alpha level is essential for hematopoietic stem cells. *Cell Stem Cell* 7:391–402.
39. Wurdak H, et al. (2010) A small molecule accelerates neuronal differentiation in the adult rat. *Proc Natl Acad Sci USA* 107:16542–16547.
40. Card PB, Erbel PJ, Gardner KH (2005) Structural basis of ARNT PAS-B dimerization: Use of a common beta-sheet interface for hetero- and homodimerization. *J Mol Biol* 353:664–677.
41. Delaglio F, et al. (1995) NMRPipe: A multidimensional spectral processing system based on UNIX pipes. *J Biomol NMR* 6:277–293.
42. Johnson BA (2004) Using NMRView to visualize and analyze the NMR spectra of macromolecules. *Methods Mol Biol* 278:313–352.
43. Jiang L, et al. (2008) De novo computational design of retro-aldol enzymes. *Science* 319:1387–1391.

Supporting Information

Partch and Gardner 10.1073/pnas.1101357108

SI Methods

Cloning and Mutagenesis. Full-length human ARNTaryl hydrocarbon nuclear translocator (ARNT) or the isolated PAS-B domain (residues 356–470) was cloned into the pcDNA4 vector (Invitrogen) with a C-terminal FLAG tag. Full-length mouse transforming acidic coiled-coil 3 (TACC3) was cloned into the pcDNA4 vector utilizing C-terminal myc-His_6 tags, with additional constructs of the isolated TACC domain (residues 427–631) and C-terminal 20 residues (CT20) truncations (residues 1–611 or 427–611). Serially truncated fragments of TACC3 for bacterial expression were cloned into the GST-parallel vector (1), along with corresponding fragments of human TACC1 (residues 661–731) and TACC2 (residues 926–996). ARNT PAS domain constructs for bacterial expression were previously described (2). All mutagenesis was performed by PCR and validated by complete sequencing.

Protein Production and Purification. Proteins were produced in phage-resistant *Escherichia coli* BL21(DE3) cells (New England Biolabs) and purified by affinity chromatography (Ni Sepharose High Performance or Glutathione Sepharose 4B, GE Healthcare) followed by size exclusion chromatography (Superdex 75, GE Healthcare). For pulldown assays, *E. coli* overexpressing GST-tagged coactivator fragments were lysed by cell extrusion and the extract was clarified by centrifugation for 30 min at 45,000 × *g* at 4 °C. Glycerol was added to 10% (v/v) and aliquots of soluble extract were quick frozen in liquid nitrogen. For NMR studies, isotopically enriched ARNT PAS-B was overexpressed in M9 minimal medium using 1 g/L ^{15}N-NH_4Cl as the sole nitrogen source (Cambridge Isotope Laboratories). Natural abundance TACC3 C-terminal peptide (residues 585–631) was purified for NMR titrations as a HisGβ1-tagged protein (3). The tag was cleaved by addition of His_6-TEV protease overnight at 4 °C (leaving a three-residue N-terminal sequence GEF); tag and protease were removed by a subsequent Ni^{2+} affinity and size exclusion chromatography. All NMR samples were buffer exchanged into 50 mM Tris pH 7.5, 20 mM NaCl, 5 mM DTT, and 10% D_2O, except for the paramagnetic relaxation enhancement (PRE) experiments, where DTT was omitted.

Cell Culture. HEK293T cells were cultured in Dulbecco's modified Eagle's medium supplemented with 10% fetal bovine serum, 2 mM L-glutamine, 100 U/mL penicillin, and 100 μg/mL streptomycin. Stabilization of endogenous HIF-1α was achieved by treatment with 200 μM $CoCl_2$ for 16 h prior to harvesting. Plasmids were transfected into cells using Lipofectamine 2000 (Invitrogen) following the manufacturer's instructions. TACC3 shRNA hairpin vectors were purchased from Open Biosystems. shRNA sequences are as follows (hairpin sequences are underlined): #1 5′ CCG<u>GGCAGTCCTTATACCTCAAGTT</u>CTCGA-G<u>AACTTGAGGTATAAGGACTGC</u>; #2 5′ CCG<u>GGCTTGTG-GAGTTCGATTTCTT</u>CTCGAG<u>AAGAAATCGAACTCCACA-AGC</u>. The nonsilencing control shRNA vector was purchased from Santa Cruz Biotechnology. Cells were harvested in 50 mM Tris pH 7.5, 150 mM NaCl, 1 mM Na_3VO_4, 10 mM NaF, 0.5% NP-40, and EDTA-free protease inhibitors (Roche). Clarified lysate was used for immunoprecipitation or luciferase assays. For immunoprecipitation, 2 mg cell lysate was incubated 1 μg antibody together with Protein A/G Plus beads (Santa Cruz Biotechnology) overnight at 4 °C. Beads were washed three times with 50 mM Tris pH 7.5, 150 mM NaCl, 0.05% NP-40 and eluted with 2× SDS buffer. Bound proteins were resolved by SDS-PAGE, transferred to polyvinylidene difluoride membranes (GE Healthcare), and immunoblotted using the following antibodies: anti-ARNT (A-3), anti-TACC3 (T-17), anti-HIF-1α (H-206), anti-GAL4 (DBD), anti-HA (Y-11), and anti-goat IgG-HRP antibodies (Santa Cruz Biotechnology); anti-mouse IgG-HRP, and anti-rabbit IgG-HRP antibodies (Sigma); and anti-His_6 antibody (Abgent). For *VEGF* HRE:luc reporter assays, cells were harvested in GLO Lysis buffer and assayed with an equal volume of Bright GLO reagent (Promega). Data represent triplicate experiments of duplicate samples, shown with SD.

mRNA Quantification. Total RNA was extracted from cells using Trizol (Invitrogen) according to the manufacturer's instructions. cDNA was synthesized from 1 ug RNA using the iScript cDNA Synthesis kit (Bio-Rad) and gene expression was analyzed from 1 μg cDNA by quantitative PCR using iTaq SYBR green Supermix with ROX on a CFX96 Real Time System (Bio-Rad). Sequences for quantitative PCR (QPCR) primer sets are as follows: *BNIP3* (NM_004043) For: 5′ TGGACGGAGTAGCTC-CAAGAG, Rev: 5′ CCGACTTGACCAATCCCATATC; *CypB* (NM_000942) For: 5′ ATGCTGCGCCTCTCCGAACG, Rev 5′ AGACCAAAGATCACCCGGCCTAC; *DEC2* (AB044088) For 5′ GCATGAAACGAGACGACACCA, Rev 5′ TGCTCGGTTA-AGGCGGTTAAA; *GLUT1* (NM_006516) For 5′ CTTTTCTGT-TGGGGGCATGAT, Rev 5′ CCGCAGTACACACCGATGAT; *PGK1* (NM_000291) For 5′ AGTCGGTAGTCCTTATGAGCC, Rev 5′ TTCCCAGAAGCATCTTTTCCC; *TACC3* (NM_006342) For 5′ CCAAGTCTGGTTGCAGTGAGGCC, Rev 5′ GCTCTC-TGCTGTTGGGGTCTCG. The results of triplicate experiments are expressed as $2^{(-\Delta\Delta C_t)}$ with SE shown, where the average Ct of the gene of interest after treatment was normalized to the reference gene, *Cyclophilin B*, and compared to a normalized, untreated sample for fold change.

NMR Spectroscopy. NMR experiments were conducted at 25 °C using a Varian INOVA 600-MHz spectrometer equipped with ^1H, ^{13}C, ^{15}N triple resonance, *Z*-axis pulsed field gradient probes. Differential broadening analysis of $^{15}N/^1H$ HSQC experiments for TACC3 binding and paramagnetic relaxation enhancement were carried out as before (2), using chemical shift assignments of wild-type ARNT PAS-B (4) and peak intensities of 150 μM ^{15}N ARNT PAS-B in the presence of 150 μM TACC3-CT. Protein for PRE experiments was obtained by mutagenesis at two independent sites using HisGβ1-tagged TACC3 C621A (res. 585–631) to generate M598C/C621A or M605C/C621A, and purified as above. Proteins were derivatized with S-cysteaminyl-EDTA (Toronto Research Chemicals) under nonreducing conditions overnight at 4 °C and further purified by size exclusion chromatography. Divalent cations (Ca^{2+} or Mn^{2+}) were coordinated at slight stoichiometric excess (1:1.1) and the protein was treated with 10 mg Chelex 100 resin for 10 min (Sigma) to remove contaminating divalent cations. PRE data were collected with paramagnetic (Mn^{2+}), diamagnetic (Ca^{2+}), or metal-free samples of EDTA-derivatized TACC3 M598C/C621A and M605C/C621A. NMR data were processed using NMRPipe/NMRDraw (5) and analyzed with NMRViewJ (6). All molecular graphics were created using PyMOL (7).

HADDOCK Modeling. A TACC3 C-terminal peptide (residues 601–631) was modeled as a parallel coiled-coil dimer using Rosetta (8). Complexes with the crystallographic ARNT PAS-B/HIF-2α PAS-B heterodimer [Protein Data Bank (PDB) ID code 3F1P

(9)] were docked using the HADDOCK 2.0 Web server (10); complexes were also docked using NMR ensemble [PDB ID code 1XO0 (4)] and crystallographic (PDB ID code 2B02) structures of the isolated ARNT PAS-B with similar results. Active residues to guide the docking were chosen on the basis of chemical shift perturbation, mutagenesis, and pulldown data, with solvent accessible passive residues automatically defined by the program. Active residues for ARNT PAS-B included 369, 370, 395, 397, 398, 409, 417, and 430. Active residues for TACC3 included 615, 616, 619, 622, 623, 626, and 630. The protocol for docking and refining followed default parameters, including semiflexible simulated annealing of all proteins in the 200 lowest-intermolecular energy solutions followed by refinement in explicit water. For each of the calculations, between 110–125 structures (out of 200) clustered into a single, low energy group with the same conformation.

1. Sheffield P, Garrard S, Derewenda Z (1999) Overcoming expression and purification problems of RhoGDI using a family of "parallel" expression vectors. *Protein Expres Purif* 15:34–39.
2. Partch CL, Card PB, Amezcua CA, Gardner KH (2009) Molecular basis of coiled coil coactivator recruitment by the aryl hydrocarbon receptor nuclear translocator (ARNT). *J Biol Chem* 284:15184–15192.
3. Harper SM, Neil LC, Gardner KH (2003) Structural basis of a phototropin light switch. *Science* 301:1541–1544.
4. Card PB, Erbel PJ, Gardner KH (2005) Structural basis of ARNT PAS-B dimerization: Use of a common beta-sheet interface for hetero- and homodimerization. *J Mol Biol* 353:664–677.
5. Delaglio F, et al. (1995) NMRPipe: A multidimensional spectral processing system based on UNIX pipes. *J Biomol NMR* 6:277–293.
6. Johnson BA (2004) Using NMRView to visualize and analyze the NMR spectra of macromolecules. *Methods Mol Biol* 278:313–352.
7. Schrödinger LLC (2010) The PyMOL Molecular Graphics System, Version 1.3, (Schrödinger LLC, New York).
8. Jiang L, et al. (2008) De novo computational design of retro-aldol enzymes. *Science* 319:1387–1391.
9. Scheuermann TH, et al. (2009) Artificial ligand binding within the HIF2alpha PAS-B domain of the HIF2 transcription factor. *Proc Natl Acad Sci USA* 106:450–455.
10. de Vries SJ, van Dijk M, Bonvin AM (2010) The HADDOCK web server for data-driven biomolecular docking. *Nat Protoc* 5:883–897.

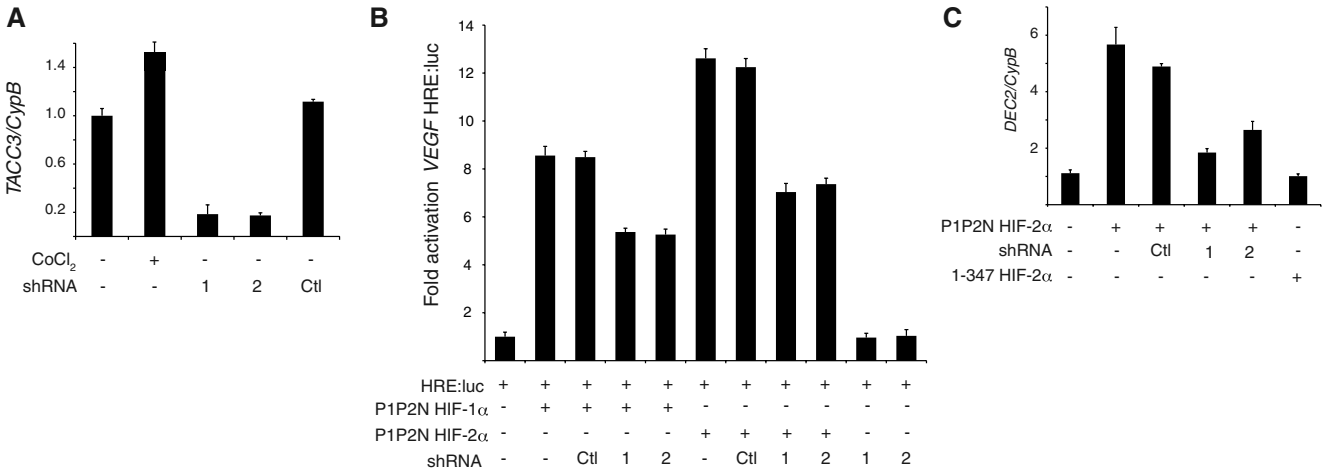

Fig. S1. *TACC3 activates transactivation of HIF-1 and HIF-2 complexes*. (*A*) Immunoblot analysis of whole-cell lysates for TACC3 expression from 293T cells harvested after $CoCl_2$ (200 μM, 16 h) or transfected with shRNA vectors (48 h). (*B*) Luciferase activity of 293T whole-cell lysates 48 h after transfection with indicated plasmids. (*C*) QPCR analysis of *DEC2* expression in 293T cells 48 h after transfection with indicated plasmids. Error bars, SD for $n = 3$ independent biological replicates.

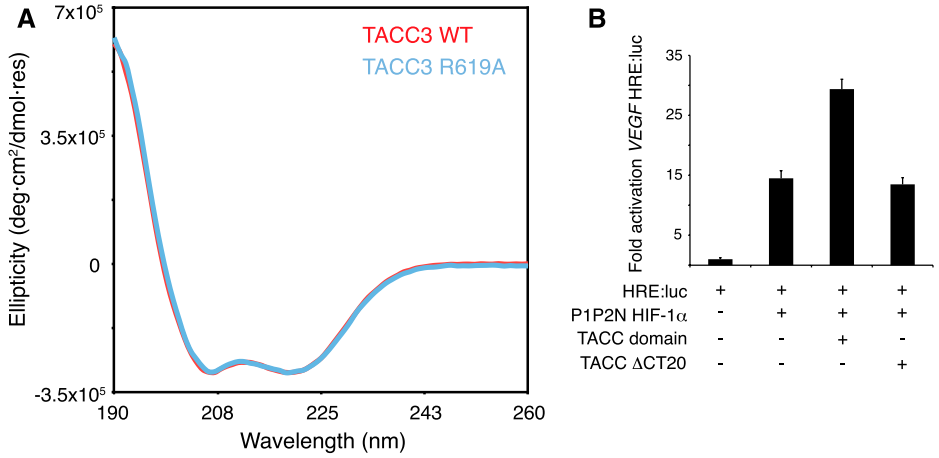

Fig. S2. *TACC3 CT20 mediates interaction with ARNT PAS-B.* (*A*) Circular dichroism spectra were collected on purified TACC3 fragments used in pulldown assays, including residues 561–631 (with the GST fusion tag removed by TEV cleavage). Spectra were recorded on 15 μM protein in 10 mM sodium phosphate, 50 mM NaCl, pH 7.0 at 25 °C on an Aviv 62DS spectropolarimeter using a 0.1-cm path-length cuvette, recording every 1 nm from 190 to 260 nm. The reference signal from buffer was subtracted from all spectra, which represent the mean of three independent scans. Molar residue ellipticities were calculated from raw ellipticities (mdeg) using the following equation:

$$\text{deg}\bullet\text{cm}^2/\text{dmol}\bullet\text{res}(\Theta) = (\text{mdeg})[\text{protein}\,(\text{M})]^{-1}\bullet(0.1\text{ cm})^{-1}\bullet(10\text{ dmol})^{-1}\bullet(\#\,\text{residues})^{-1}$$

Coiled-coil structure was assessed by monitoring minima at 208 and 222 nm, where a value ≈ 1.0 is indicative of coiled coil (1). (*B*) Luciferase activity of 293T whole-cell lysates 48 h after transfection with indicated plasmids.

1. Graddis TJ, Myszka DG, Chaiken IM (1993) Controlled formation of model homo- and heterodimer coiled coil polypeptides. *Biochemistry* 32:12664–12671.

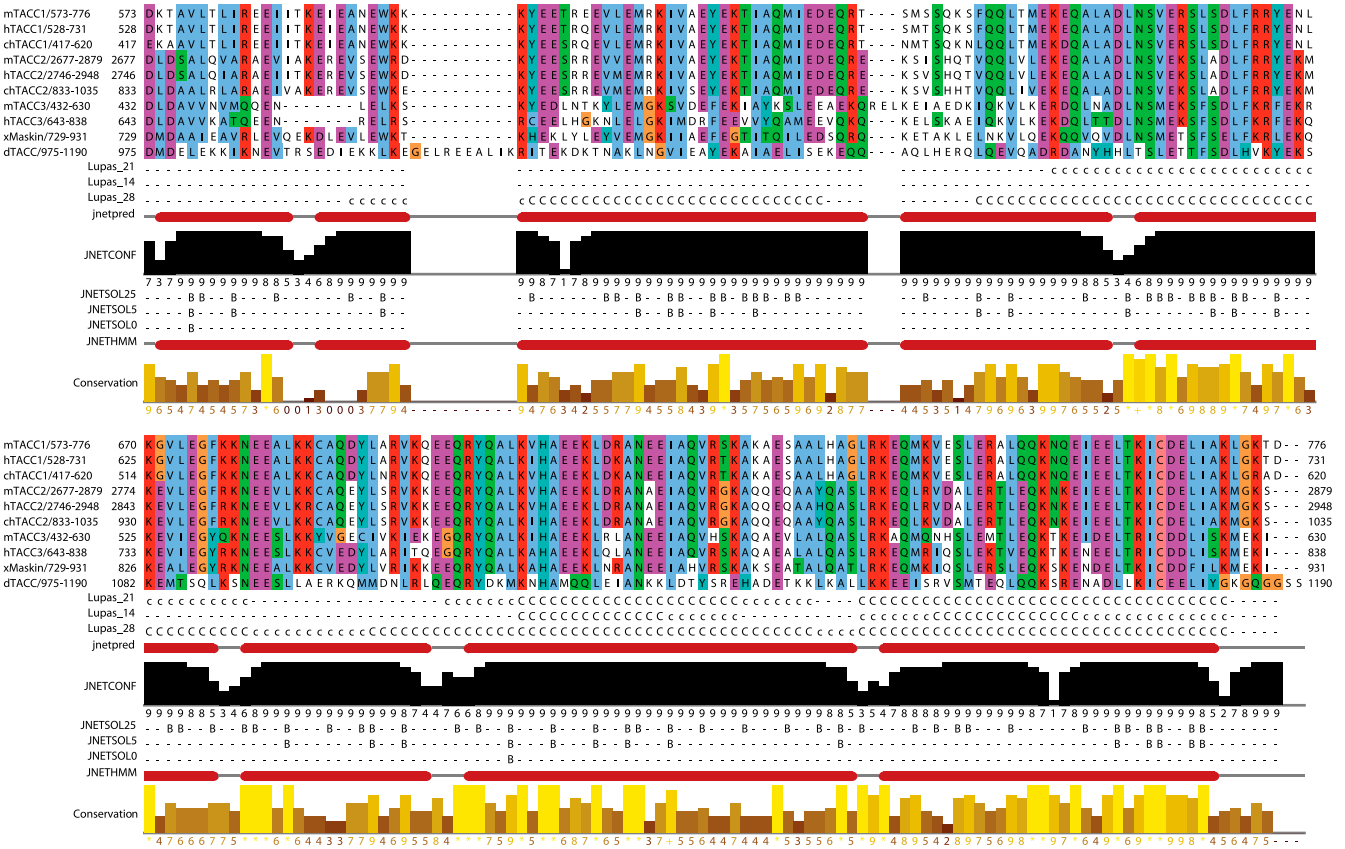

Fig. S3. *The TACC domain is highly conserved within the TACC family.* TACC domains from mouse (m), human (h), chicken (ch), xenopus (x), and *Drosophila* (d) TACC proteins were aligned with domain boundaries as indicated using Jalview (1).

1. Waterhouse AM, Procter JB, Martin DM, Clamp M, Barton GJ (2009) Jalview Version 2—A multiple sequence alignment editor and analysis workbench. *Bioinformatics* 25:1189–1191.

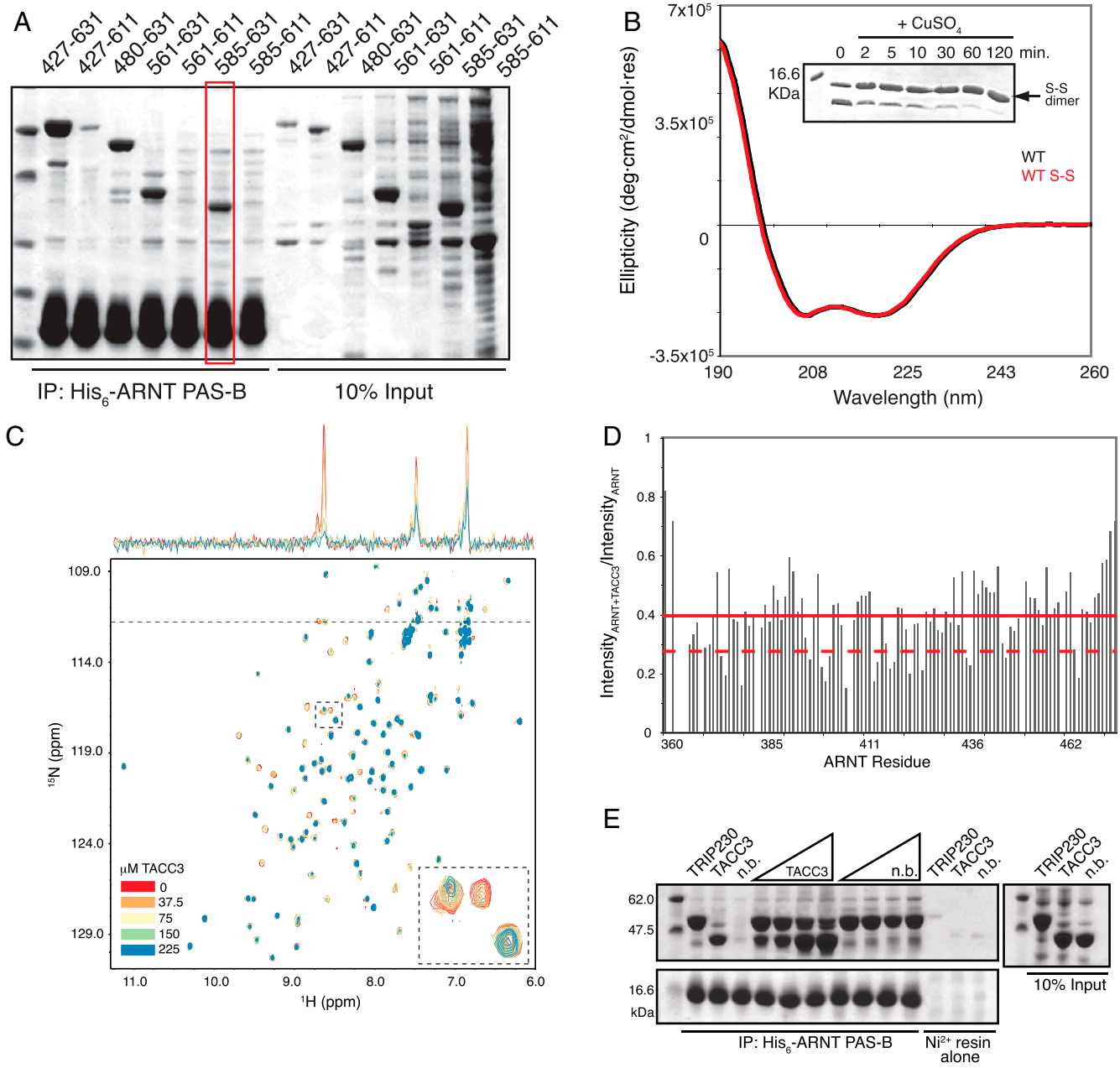

Fig. S4. *Biochemical, structural, and sequence analyses of the ARNT-binding region of TACC3.* (*A*) Pulldown assay of His_6-tagged ARNT PAS-B and TACC3 fragments including the minimal fragment used for NMR studies (residues 585–631, red box). (*B*) CD spectrum of 15 μM TACC3 (585–631) with or without disulfide cross-linking through the native cysteine at residue 621 (position a within the heptad repeat) in 10 mM sodium phosphate, 50 mM NaCl, pH 7.0 at 25 °C. (*Inset*) Oxidation of native cysteines was induced by addition of 50 μM $CuSO_4$ to 200 μM protein at 25 °C. Samples were taken at the indicated time points and quenched in SDS buffer with 100 mM EDTA. Cross-linking was monitored by 20% SDS-PAGE and Coomassie staining. (*C*) $^{15}N/^{1}H$ HSQC experiment of ^{15}N ARNT PAS-B titrated with natural abundance TACC3 at the indicated concentrations. (*Inset*) Close-up view of broadened residues. Dashed horizontal line represents location of a 1D trace at this ^{15}N chemical shift displaying peak intensities as a function of TACC3 titration (above). (*D*) Differential broadening analysis of ^{15}N ARNT PAS-B peak intensities in the presence of 225 μM of each TACC3 and apo ^{15}N ARNT PAS-B. Solid red line indicates mean intensity of all ARNT peaks; dashed red line indicates the 1σ cutoff. (*E*) Pulldown assay of His_6-ARNT PAS-B with GST-tagged coativator fragments, including a nonbinding control fragment from TRIP230(2)[6] (residues 1663–1716). Competition for GST-TRIP230 binding in the pulldown assay was assessed in the presence of 1, 3, 6, and 9× volumes of either GST-TACC3 or the GST-tagged nonbinding fragment relative to the input volume of GST-TRIP230.

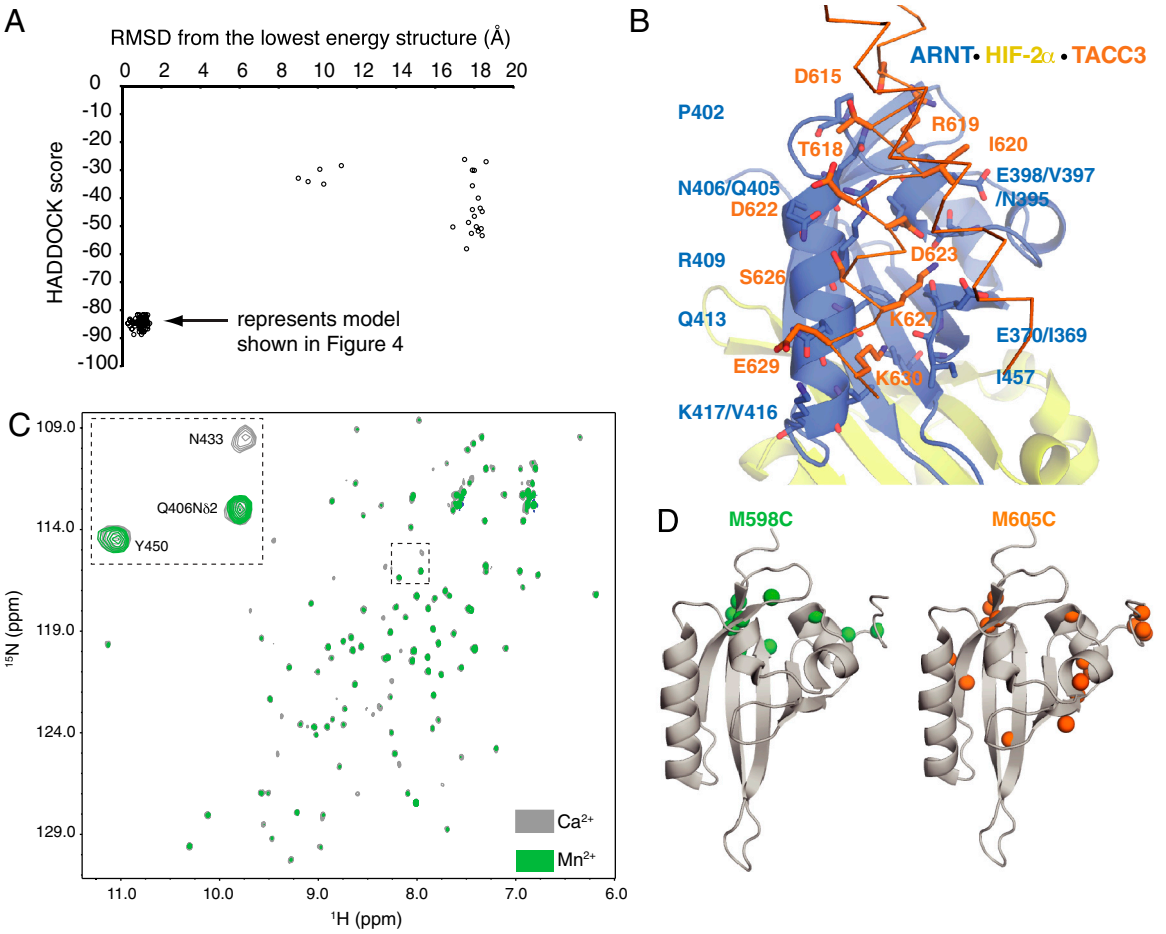

Fig. S5. *Scoring and validation of HADDOCK-derived ternary complex*. (*A*) HADDOCK score vs. rmsd (Å) from lowest energy structure. HADDOCK model shown in Fig. 4 represents 115 of the top 150 lowest energy structures, indicated with an arrow. (*B*) Ribbon diagram of TACC3/ARNT/HIF-2α complex showing residues involved at interface. Cartoon representations of ARNT (blue) and HIF-2α (yellow) PAS-B domains are along with the two TACC3 (orange) chains are shown as Cα traces. Side chains of residues at the ARNT/TACC3 interface are depicted as sticks. The two views differ by a 90° rotation around the vertical axis. (*C*) $^{15}N/^{1}H$ HSQC experiment of ^{15}N ARNT PAS-B with EDTA-derivatized TACC3 (M598C) chelated with either Ca^{2+} (gray) or Mn^{2+} (green) to assess Mn^{2+}-dependent paramagnetic relaxation enhancement on ARNT PAS-B. (*Inset*) Close-up view of Mn^{2+}-dependent broadening. (*D*) Significantly broadened amide protons (spheres) from PRE experiments with M598C (green) and M605C (orange) mapped onto the ARNT PAS-B structure [PDB ID code 1XO0; (4)].

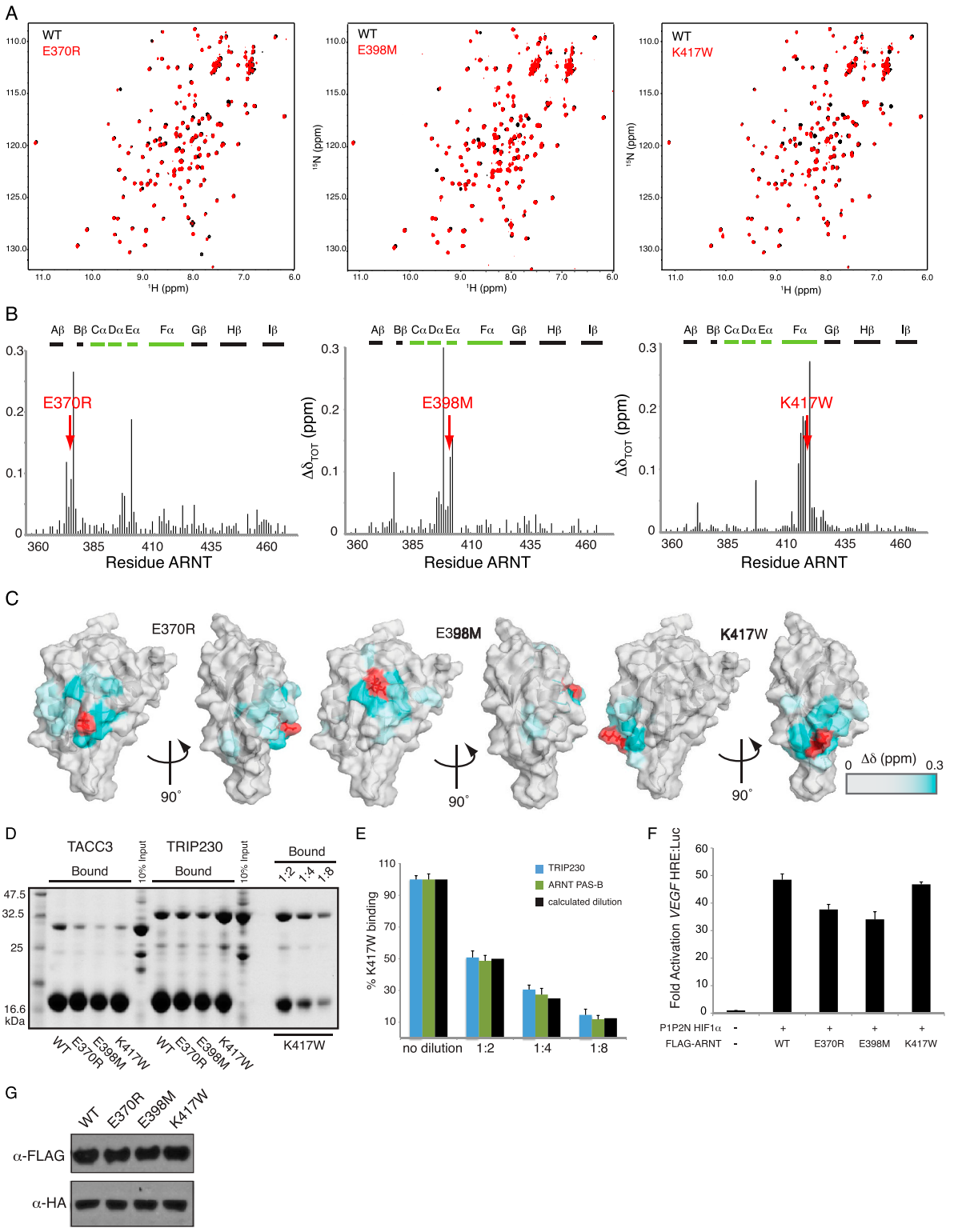

Fig. S6. *Analysis of ARNT PAS-B mutant protein interactions and structures.* (*A*) ^{15}N/^{1}H HSQC spectra of WT (black) and mutant (red) ^{15}N His$_6$-ARNT PAS-B proteins. (*B*) Chemical shift perturbations due to PAS-B mutation were quantitatively measured as in (1). Secondary structure elements are depicted schematically above the data; black bars represent the location of β-sheet secondary structure, whereas the green bars represent the α-helices of the PAS-B domain. The location of the mutation is indicated with a red arrow. (*C*) Chemical shift perturbations due to mutations heat-mapped onto the ARNT PAS-B structure [PDB ID code 1XO0; (2)]. (*D*) Full gel of pulldown assay shown in Fig. 5*B* with serial dilution of bound His$_6$-ARNT PAS-B (K417W)/GST-TRIP230 to verify accurate quantification by densitometry. (*E*) Densitometric analysis of bound GST-TACC3 or GST-TRIP230 with His$_6$-ARNT PAS-B WT and mutants from Ni-pulldown assay. (*F*) Luciferase activity of 293T whole-cell lysates 48 h after transfection with indicated plasmids. (*G*) Immunoblot analysis of whole-cell lysates from a representative QPCR experiment (i.e., Fig. 5*D*).

1. Partch CL, Card PB, Amezcua CA, Gardner KH (2009) Molecular basis of coiled coil coactivator recruitment by the aryl hydrocarbon receptor nuclear translocator (ARNT). *J Biol Chem* 284:15184–15192.
2. Card PB, Erbel PJ, Gardner KH (2005) Structural basis of ARNT PAS-B dimerization: Use of a common beta-sheet interface for hetero- and homodimerization. *J Mol Biol* 353:664–677.

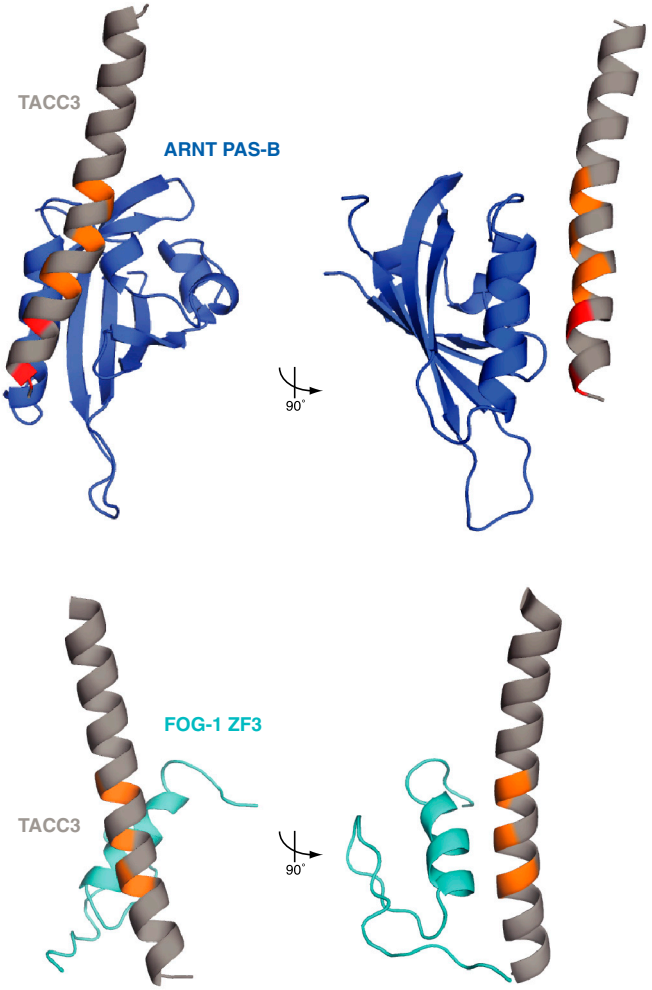

Fig. S7. *Structural comparison of the TACC3 CT20 interaction with ARNT PAS-B and the FOG-1 (friend of GATA-1) Zinc Finger 3 domain (ZF3)* (1). TACC3 residues involved in ARNT PAS-B and FOG-1 ZF3 binding (sites 1, 2, and 3; Fig. 2) are shown in orange, whereas those in the C-terminal 6 residues that are important for ARNT PAS-B binding are shown in red. The second helix of the coiled coil has been omitted for the sake of clarity.

1. Simpson RJ, et al. (2004) A classic zinc finger from friend of GATA mediates an interaction with the coiled-coil of transforming acidic coiled-coil 3. *J Biol Chem* 279:39789–39797.

Other Supporting Information Files

Dataset S1 (PDB)